Sturgill et al., http://www.jcb.org/cgi/content/full/jcb.201507036/DC1

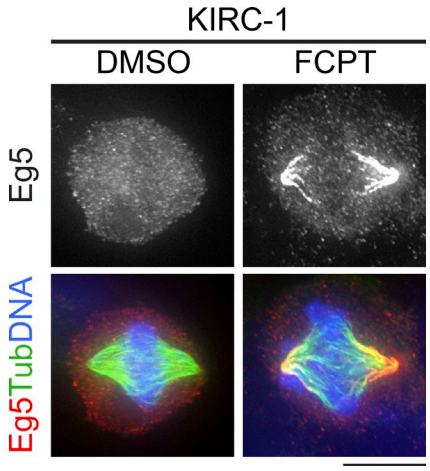

Figure S1. **The Eg5 mechanochemical state induced by rigor is dominant to the effects of STLC.** Maximum intensity z-projections of KIRC-1 cells treated with DMSO or FCPT and stained with antibodies targeting Eg5 (grayscale as individual and red in merge) and tubulin (green). DNA, blue. LUTs for grayscale and red channels are scaled identically. Bar, 10 µm.

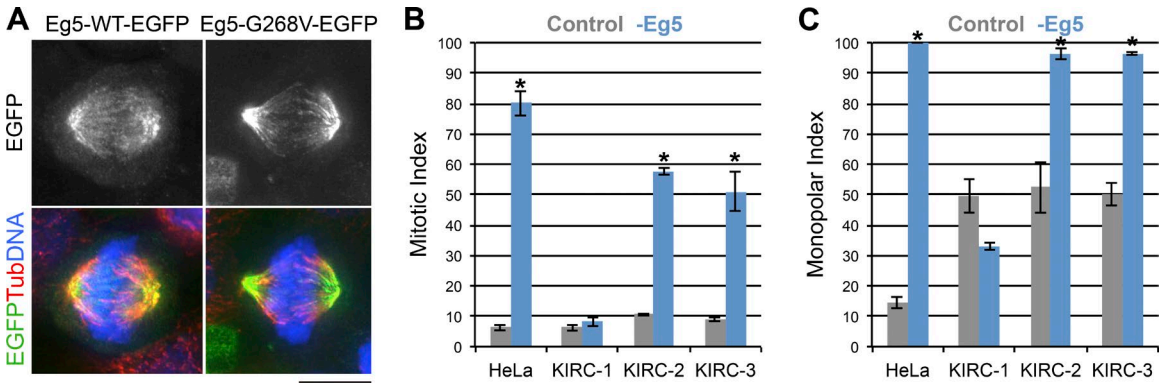

Figure S2. **Exogenous expression of Eg5-G268V-EGFP in mitotic cells and quantitation of the MI and MPI in Eg5-depleted cells.** (A) Exogenous Eg5-G268V-EGFP induces spindle MT bundling. Maximum intensity z-projections of mitotic HeLa cells expressing Eg5-WT-EGFP or Eg5-G268V-EGFP (grayscale and green) and stained with antibodies targeting tubulin (red). LUTs for individual channels are scaled identically. Bar, 10 µm. B) Eg5 depletion induces a mitotic arrest in KIRC-2 and -3. Values represent the mean MI of indicated cell types 1 d after transfection with nontargeting (gray) or Eg5-targeting (blue) siRNAs. Error bars, ± SEM; $n \geq 345$ cells from three independent experiments; *, $P \leq 0.03$ relative to control. (C) Eg5 depletion prevents spindle assembly in KIRC-2 and -3. Values represent the mean MPI of indicated cell types 1 d after transfection with nontargeting (gray) or Eg5-targeting (blue) siRNAs. Error bars, ± SEM; $n = 300$ cells from three independent experiments; *, $P \leq 0.03$ relative to control.

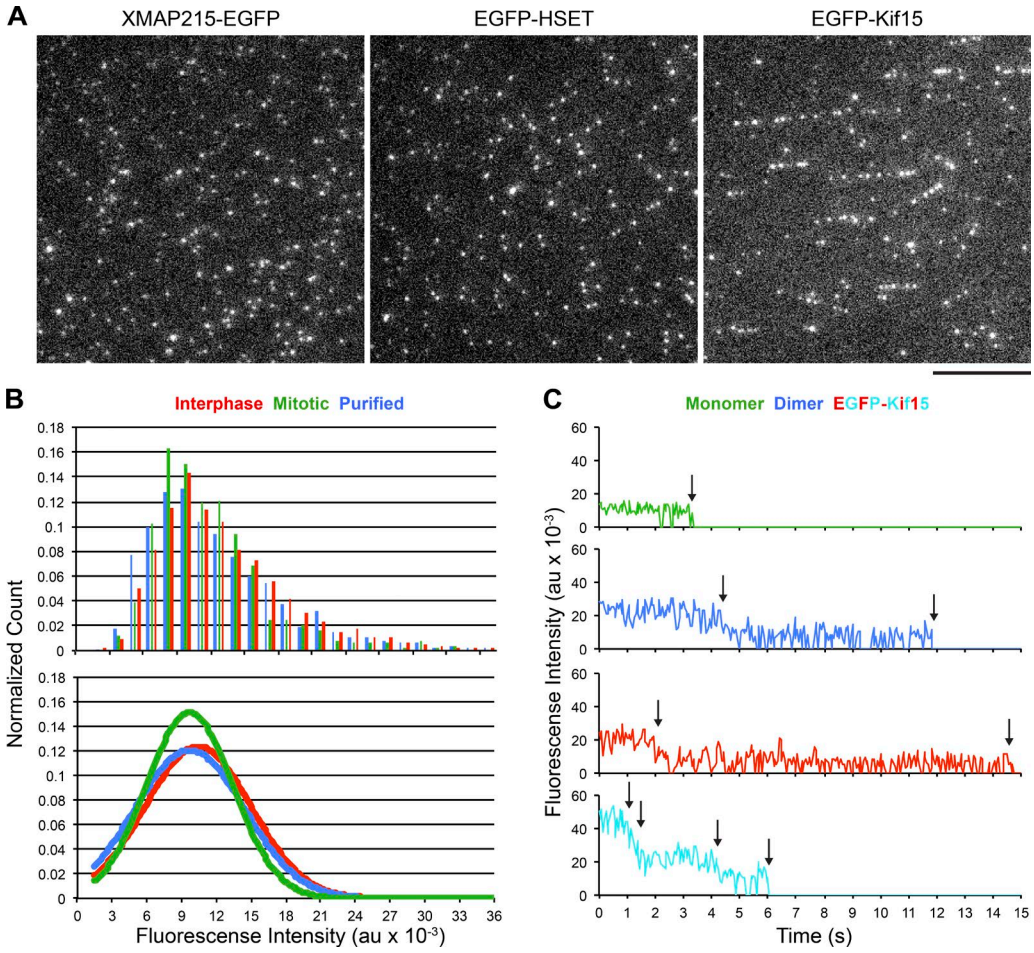

Figure S3. **Representative fields of view from single-molecule imaging experiments and initial fluorescence intensities of EGFP-Kif15 from interphase and mitotic cell extracts.** (A) Initial frames from time-lapse photobleaching experiments showing flow cells infused with XMAP215-EGFP, EGFP-HSET, or EGFP-Kif15 as indicated. XMAP215-EGFP and EGFP-HSET were nonspecifically bound, whereas EGFP-Kif15 molecules were bound to surface-bound MTs with AMPPNP. Bar, 10 µm. (B) Cellular Kif15 primarily organizes into dimers regardless of cell cycle state. (top) Histogram showing initial fluorescence intensities of EGFP-Kif15 from interphase HeLa cell extracts (red, 10,801 ± 282 au, mean ± 95% COI) and mitotic HeLa cell extracts (green, 9,673 ± 428 au, mean ± 95% COI). Purified EGFP-Kif15 (blue, 10,334 ± 282 au, mean ± 95% COI) is also shown. Counts are normalized to 1. n = 1,985 (interphase), 482 (mitotic), and 1,652 (purified) particles from ≥9 fields of view. (bottom) Single Gaussian fits of fluorescence intensity distributions shown above. Interphase (red, R^2 = 0.92), mitotic (green, R^2 = 0.94), and purified (blue, R^2 = 0.90). Fluorescence intensities are indicated in au × 10^{-x}. (C) Traces from Fig. 3 E displayed on separate plots. XMAP215-EGFP (green) represents monomer control. EGFP-HSET (blue) represents dimer control. Two example traces are shown for EGFP-Kif15 (red and cyan). Arrows denote probable photobleaching steps. Fluorescence intensities are indicated in au × 10^{-x}, and the baseline is set to the background fluorescence.

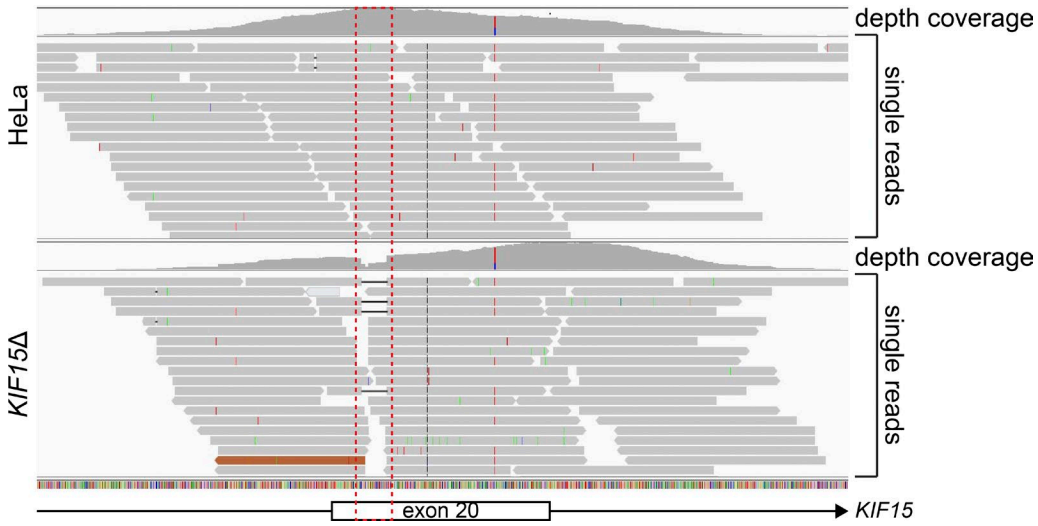

Figure S4. **Integrative Genomics Viewer showing disruption of *KIF15* exon 20 in the *KIF15*Δ line.** Depth coverage and single reads from WES of HeLa (top) and *KIF15*Δ (bottom) genomic DNA around *KIF15* exon 20. The red stippled box highlights the area of CRISPR-mediated genomic alteration in the *KIF15*Δ line, appearing as a decrease in depth coverage and gaps in the single reads.

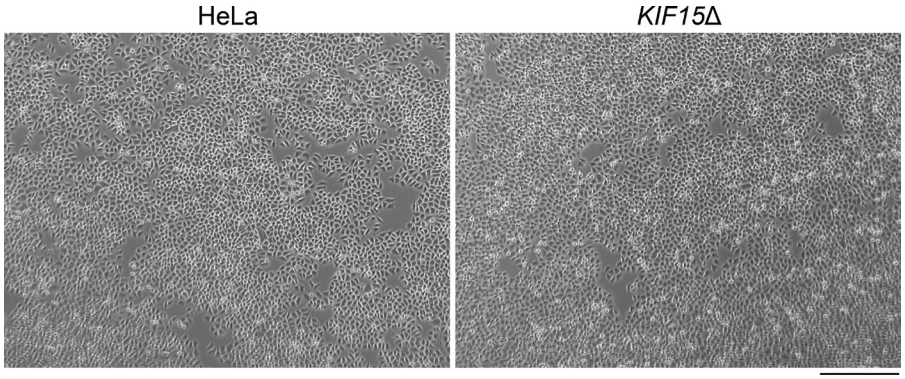

Figure S5. **Plating of HeLa and *KIF15*Δ cells for long-term K5I-resistance experiments.** Bright-field images of HeLa and *KIF15*Δ cells 1 d after plating at 6.8 ± 10^6 cells per 10-cm dish. Bar, 500 µm.

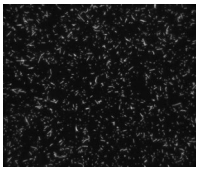

Video 1. **Time-lapse imaging of X-rhodamine–labeled MT gliding powered by Eg5-WT.** Acquisition at 5-s intervals, with playback at five frames per second.

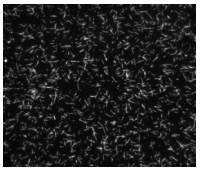

Video 2. **Time-lapse imaging of X-rhodamine–labeled MT gliding powered by Eg5-G268V.** Acquisition at 5-s intervals, with playback at five frames per second.